EFFECT OF CREEP-FATIGUE LOADING CONDITION ON CRACK TIP FIELDS OF GRADE 91 STEEL AT CRACK INITIATION AND GROWTH

Hyun-Woo Jung[1], Yun-Jae Kim[1], and Yukio Takahashi[2]

[1]Korea University
[2]Central Research Institute of Electric Power Industry

November 10, 2020

Abstract

In this paper, the effect of creep-fatigue loading condition on crack tip deformation and stress fields of Grade 91 steel at 600oC at crack initiation and growth is studied. By using finite element debond analysis method, creep-fatigue crack growth tests using C(T) specimens under various load ratios and hold times are simulated, and the effect of creep-fatigue load ratio and hold time on the plastic zone, creep zone, crack opening profile, equivalent stress, crack-opening stress and triaxiality at crack initiation and growth is presented. It is found that the crack tip deformation and stress fields under tension-compression creep-fatigue loading are overall different from those under tension-tension creep-fatigue and pure creep loading, due to crack closure.

Effect of Creep-fatigue Loading Condition on Crack Tip Fields of Grade 91 Steel at Crack Initiation and Growth

Hyun-Woo Jung[1], Yun-Jae Kim[1]*,

[1] Korea University, Department of Mechanical Engineering

145, Anam-ro, Sungbuk-gu, Seoul, 02841, Korea

Yukio Takahashi[2]

[2] Central Research Institute of Electrical Power Industry

2-6-1, Nagasaka, Yokosuka-shi, Kanagawa, 240-0196, Japan

* Corresponding author: (E-Mail) kimy0308@korea.ac.kr

Manuscript for

Fatigue and Fracture of Engineering Materials and Structures

Submission Date: November 10, 2020

ABSTRACT

In this paper, the effect of creep-fatigue loading condition on crack tip deformation and stress fields of Grade 91 steel at 600°C at crack initiation and growth is studied. By using finite element debond analysis method, creep-fatigue crack growth tests using C(T) specimens under various load ratios and hold times are simulated, and the effect of creep-fatigue load ratio and hold time on the plastic zone, creep zone, crack opening profile, equivalent stress, crack-opening stress and triaxiality at crack initiation and growth is presented. It is found

that the crack tip deformation and stress fields under tension-compression creep-fatigue loading are overall different from those under tension-tension creep-fatigue and pure creep loading, due to crack closure.

Keywords: creep fatigue, crack initiation, crack growth, crack tip stress fields

NOMENCLATURE

a, a_0 crack length and its initial value

$\boldsymbol{\alpha}$ back stress tensor

B_N net thickness of specimen

C^* C^* -integral

Δa crack growth length

E Young's modulus

ϵ strain

ϵ_{ς} creep strain

$\epsilon_{\pi\varsigma}$, $\epsilon_{\sigma\varsigma}$ primary and secondary creep strain

$\varepsilon^{p}_{\mathrm{ref}}$,$\dot{\varepsilon}^{c}_{\mathrm{ref}}$ reference plastic and creep strain

m strain hardening exponent

n creep exponent

N_f cycles to failure

J J -integral

p equivalent plastic strain

P_0 plastic limit load

P_{max}, P_{min} applied maximum and minimum load

R load ratio (P_{min} /P_{max})

σ stress

σ stress tensor

σ_0 yield strength

$\sigma_{\rho\epsilon\varphi}$ reference stress

$\sigma^{\mathrm{RR}}_{\mathrm{ij}}$ RR field

$\tilde{\sigma}_{\mathrm{ij}}$ dimensionless stress function

$\sigma^{0}{}_{\psi}$ yield strength at zero plastic strain

t_h creep-fatigue hold time

t_{fp} end of primary creep time

W width of the specimen

ABBREVIATION

ASTM American Society for Testing and Materials

ASME American Society of Mechanical Engineers

C(T) Compact Tension

FE Finite Element

RR Riedel and Rice

Sp. Specimen

1. INTRODUCTION

In assessing structural integrity of high-temperature power-plant components, it is essential to understand crack initiation and growth behaviour under creep and creep-fatigue loadings. High-temperature crack initiation and growth behaviours of a Grade 91 steel under constant load have been investigated by many researchers [1-10]. It is known that the creep crack initiation time and growth rate can be correlated with the time-dependent fracture mechanics C^* -integral [11-18]. Under creep-fatigue cyclic loading condition, the interaction of creep and fatigue is involved in the crack initiation and growth. Creep-fatigue crack growth tests have been extensively performed [3, 19-29], but most of the tests were conducted under tension-tension creep-fatigue loading condition [3, 21-27, 29]. On the other hand, creep-fatigue crack growth tests under tension-compression creep-fatigue loading are limited [19-20, 28].

The previous study [28] showed that the crack growth rate under tension-tension creep fatigue loading was generally well correlated by the C^* parameter, but that under tension-compression creep-fatigue loading was overestimated by the conventional approach using the C^*parameter. To fully understand the singularity of the crack growth behavior under tension-compression creep-fatigue loading, the effect of creep-fatigue loading condition on crack tip deformation, stress and strain fields should be studied, but previous studies [30-39] were only for pure fatigue loading condition, not for creep-fatigue loading condition.

In this study, creep-fatigue crack growth tests of Grade 91 steel at 600°C using the compact tension specimens under various load ratios and hold times [28] are simulated by using finite element debond analysis to investigate the effect of creep-fatigue loading condition on crack tip deformation and stress fields at crack initiation and growth. Section 2 presents the creep-fatigue creep growth test data used in this study. Section 3 describes the FE analysis. The effect of creep-fatigue loading condition on crack tip deformation and stress fields at crack initiation and growth is presented in Section 4. Section 5 concludes the presented work.

2. SUMMARY OF CREEP-FATIGUE CRACK GROWTH TESTS

Creep-fatigue crack growth tests of Grade 91 at 600°C under various load ratios and hold times were performed using compact tension (C(T)) specimens to investigate crack growth behavior under fully reversed creep-fatigue cyclic loading condition [28]. The C(T) specimen had the thickness of 20 mm, net thickness of 16 mm and width of 50mm. Chemical composition of the tested material is given in Table 1, together with those of other similar materials, ASME Grade 91 [40] and European X10CrMoVNb9-1 [41]. Material properties of these similar materials will be used for analysis in this paper.

Creep-fatigue crack growth test conditions for three tests are schematically shown in Fig. 1 and summarized in Table 2. The plastic limit load P_0 was calculated using the following equation [42]

Hosted file

`image1.emf` available at https://authorea.com/users/374572/articles/492073-effect-of-creep-fatigue-loading-condition-on-crack-tip-fields-of-grade-91-steel-at-crack-initiation-and-growth

(1)

where a is crack length; B_N is the net thickness; W is the width; σ_0 is the yield strength of material (in this paper, σ_0 =311 MPa is used). Among the test cases, the specimen 1 having the highest load ratio would be the creep-dominant case and the specimen 5 having the shortest hold time would be the fatigue-dominant case. For the specimen 3, the creep and fatigue effect would be comparable. These three creep-fatigue crack

growth tests cases will be analysed in this paper. Test results for the crack length versus number of cycles are shown in Fig. 2(a) and for load line displacement versus number of cycles in Fig. 2(b).

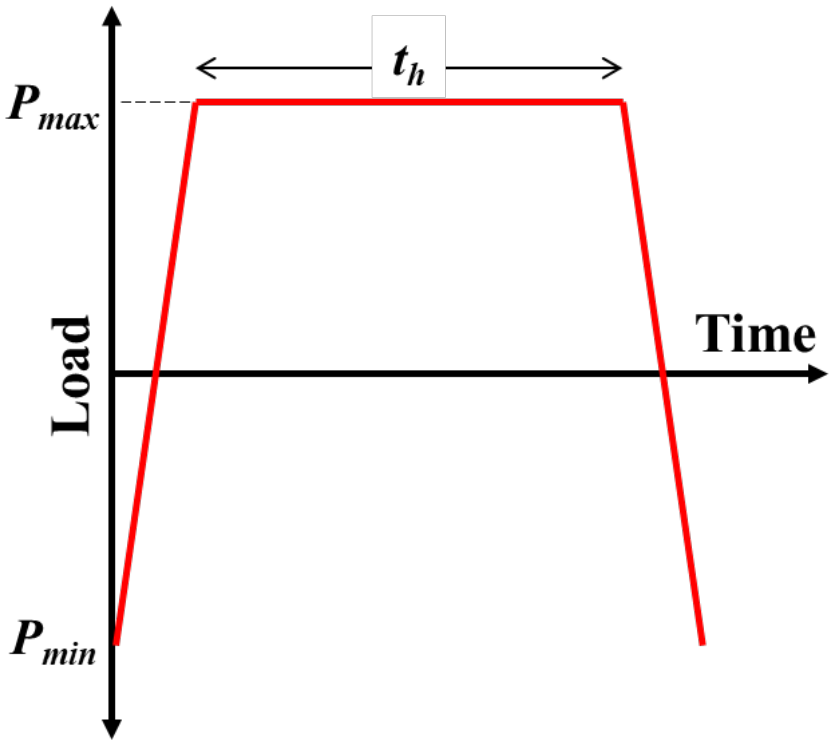

Fig. 1. Schematic illustration of creep-fatigue loading condition.

Hosted file

`image3.emf` available at https://authorea.com/users/374572/articles/492073-effect-of-creep-fatigue-loading-condition-on-crack-tip-fields-of-grade-91-steel-at-crack-initiation-and-growth

Hosted file

`image4.emf` available at https://authorea.com/users/374572/articles/492073-effect-of-creep-fatigue-loading-condition-on-crack-tip-fields-of-grade-91-steel-at-crack-initiation-and-growth

(a) (b)

Fig. 2. Creep-fatigue crack growth test data (digitized from Ref. [28]): (a) crack length versus number of cycles and (b) load line displacement versus number of cycles.

Table 1. Chemical composition of tested material (wt%) [28, 40-41].

	C	Si	Mn	P	S	Cr	Mo	V	Ni	Al	Nb	N
Y. Takahashi [28]	0.09	0.24	0.44	0.003	0.001	8.78	0.94	0.21	0.04	0.013	0.08	0

	C	Si	Mn	P	S	Cr	Mo	V	Ni	Al	Nb	N
Grade 91 Specification [40]	0.08	0.20	0.30	...	...	8.00	0.80	0.18	...	...	0.06	.
	0.12	0.50	0.60	0.020	0.010	9.50	1.05	0.25	0.40	0.04	0.10	.
X10CrMoVNb9-1 Specification [41]	0.08	...	0.30	...	...	8.00	0.85	0.18	...	...	0.06	0
	0.12	0.50	0.60	0.025	0.015	9.50	1.05	0.25	0.40	0.03	0.10	0

Table 2. Summary of test conditions [28].

Specimen number	P_{max} (kN)	P_{min} (kN)	P_o (kN)	R (=P_{max}/ P_{min})	t_h (h)	a_0 (mm)	N_f (cycles)
1	12.0	10.0	33.5	0.833	10	23.5	131
3	12.0	-12.0	33.3	-1.000	10	23.6	121
5	12.5	-11.5	31.3	-0.920	0.167	24.3	687

3. FINITE ELEMENT ANALYSIS

3.1 FE Debond Analysis

The creep-fatigue crack growth tests explained in Chapter 2 were simulated using the ABAQUS debond analysis option [43]. Figure 3 shows the FE mesh of the C(T) specimen, consisting of 1 4,964 two-dimensional (2-D) plane strain second-order solid elements with reduced integrations (CPE8R). For loading and unloading, the static structural analysis option, *STATIC, was used and for creep-hold, the quasi-static analysis option, *VISCO, was used with the user-subroutine CREEP. The FE analysis was performed using the large geometry change option (NLGEOM in ABAQUS). To simulate crack growth, the debond option in ABAQUS was used using the *FRACTURE CRITERION, TYPE=CRACK LENGTH keyword option. The debond analysis method is schematically described in Fig. 4, where the experimentally-measured crack extension data were given as a function of time using the crack length criteria. The crack advances according to the crack length input by releasing nodes. Outputs were the load-line displacement, crack tip stress and strain fields.

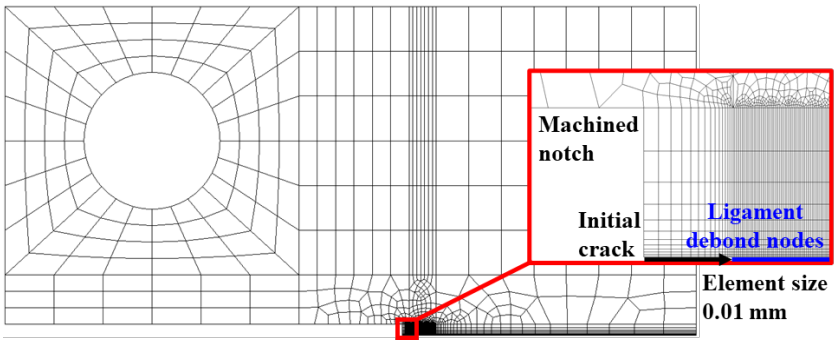

Figure 3. 2-D plane strain C(T) FE mesh for the debonding analysis

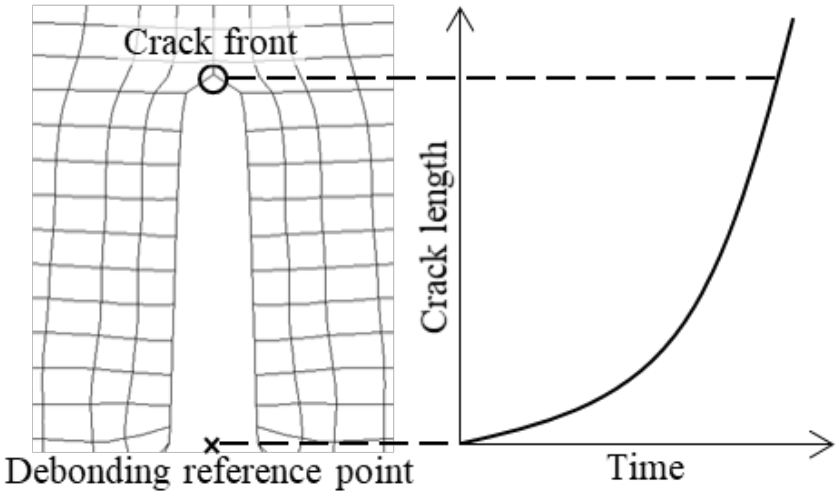

Figure 4. Schematic representation of FE debonding analysis method

3.2 Cyclic Hardening Model

For the cyclic hardening model, three hardening models were used in this paper: a kinematic hardening model determined from the tensile stress-strain curve of X10CrMoVNb9-1 from RCC-MRx [44] and two Chaboche combined hardening models [45-46] with parameters for Grade 91 at 600°C, proposed by Kyaw et al. [47] and Saad et al. [48].

The kinematic hardening model is based on the average tensile stress-strain curve of X10CrMoVNb9-1 from RCC-MRx [44], which is given below:

Hosted file

`image7.emf` available at https://authorea.com/users/374572/articles/492073-effect-of-creep-fatigue-loading-condition-on-crack-tip-fields-of-grade-91-steel-at-crack-initiation-and-growth

(2)

where ϵ is the strain in mm/mm; σ is the stress in MPa; Young's modulus E =167,000 MPa; C_0 =1.0435;$(R^t_{p0.2})_{moy}$ =288 MPa; and a =37.88.

The Chaboche combined hardening model considers both kinematic and isotropic hardening. In the combined hardening model, the yield function$F$ is defined as:

Hosted file

`image8.emf` available at https://authorea.com/users/374572/articles/492073-effect-of-creep-fatigue-loading-condition-on-crack-tip-fields-of-grade-91-steel-at-crack-initiation-and-growth

(3)

Hosted file

image9.emf available at https://authorea.com/users/374572/articles/492073-effect-of-creep-fatigue-loading-condition-on-crack-tip-fields-of-grade-91-steel-at-crack-initiation-and-growth

(4)

where σ is the stress tensor; α is the backstress tensor representing the translation of the yield surface; s is the deviatoric stress tensor; a is the deviatoric part of the backstress tensor; and σ_y^0 is the yield strength at zero plastic strain. In Eq. (3), Idescribes the expansion or contraction of the yield surface, defined as:

Hosted file

image10.emf available at https://authorea.com/users/374572/articles/492073-effect-of-creep-fatigue-loading-condition-on-crack-tip-fields-of-grade-91-steel-at-crack-initiation-and-growth

(5)

where Q and b are the isotropic hardening parameters; and$p$ is the equivalent plastic strain. The backstress tensor, α is defined as:

Hosted file

image11.emf available at https://authorea.com/users/374572/articles/492073-effect-of-creep-fatigue-loading-condition-on-crack-tip-fields-of-grade-91-steel-at-crack-initiation-and-growth

(6)

Hosted file

image12.emf available at https://authorea.com/users/374572/articles/492073-effect-of-creep-fatigue-loading-condition-on-crack-tip-fields-of-grade-91-steel-at-crack-initiation-and-growth

(7)

where N is the number of backstresses; α_k is the k-th back stress tensor;C_k and γ_κ are the kinematic hardening parameters for the k-th back stress tensor. In this study, the isotropic and kinematic hardening parameters for Grade 91 at 600°C suggested by Kyaw et al. [47] and Saad et al. [48] were used, which are summarized in Table 3. In Fig. 5, variations of the peak stress under the 1% fatigue strain range using three hardening models used in this study are compared with the experimental result by Yaguchi and Takahashi [49] for Grade 91, used for creep-fatigue crack growth test summarized in Chapter 2. The peak stress of the kinematic hardening model is constant by definition, while those of two combined hardening models decreases with the number of cycles. The peak stress of the combined hardening model by Saad et al. is generally lower than that by Kyaw et al., but the trend of cyclic softening behaviour is almost the same with each other. The model by Kyaw et al. is closest to the experimental result.

Table 3. The parameters of Chaboche combined hardening models.

	E (MPa)	${\sigma^0}_\psi$ (MPa)	Q (MPa)	b	C_1 (MPa)	γ_1	C_2 (MPa)	γ_2
Kyaw et al. [47]	128,700	214	-62.1	1.7	27,900	620	12,389	621
Saad et al. [48]	139,395	220	-75.4	1.0	106,860	2,055	31,160	463

Hosted file

image13.emf available at https://authorea.com/users/374572/articles/492073-effect-of-creep-fatigue-loading-condition-on-crack-tip-fields-of-grade-91-steel-at-crack-initiation-and-growth

Figure 5. Comparison of the peak stress variation under 1% of the fatigue strain range for three cyclic hardening models.

3.3 Creep Strain Model

For the creep constitutive model, the creep strain model for X10CrMoVNb9-1, equivalent to ASME Grade 91, at 600°C from RCC-MRx [44] was used, given by

Hosted file

image14.emf available at https://authorea.com/users/374572/articles/492073-effect-of-creep-fatigue-loading-condition-on-crack-tip-fields-of-grade-91-steel-at-crack-initiation-and-growth

(4)

where $\dot{\varepsilon}_c$ is the creep strain rate in %/hr; $\dot{\varepsilon}_{pc}$ and$\dot{\varepsilon}_{sc}$ are the primary creep strain rate in %/h and secondary creep strain rate in %/h, respectively. The primary creep strain model in RCC-MRx [44] is given by

Hosted file

image15.emf available at https://authorea.com/users/374572/articles/492073-effect-of-creep-fatigue-loading-condition-on-crack-tip-fields-of-grade-91-steel-at-crack-initiation-and-growth

(5)

where ϵ_c is the creep strain in %; σ is the stress in MPa; K= 2.9372 x 10^{-22};x =-1.7717; and y =8.8293. For zeroϵ_c (at the first increment of analysis), the primary creep strain is calculated using

Hosted file

image16.emf available at https://authorea.com/users/374572/articles/492073-effect-of-creep-fatigue-loading-condition-on-crack-tip-fields-of-grade-91-steel-at-crack-initiation-and-growth

(6)

where $\Delta\tau_i$ is initial time increment;C_1 =2.4622 x 10^{-8};C_2 =0.3608; and n_1 =3.1854. The secondary creep strain rate is given by

Hosted file

image17.emf available at https://authorea.com/users/374572/articles/492073-effect-of-creep-fatigue-loading-condition-on-crack-tip-fields-of-grade-91-steel-at-crack-initiation-and-growth

(7)

where C =6.1560 x 10^{-20}; and n =7.63. Under variable creep stresses, the creep strainϵ_s in Eq. (5) is calculated using

Hosted file

image18.emf available at https://authorea.com/users/374572/articles/492073-effect-of-creep-fatigue-loading-condition-on-crack-tip-fields-of-grade-91-steel-at-crack-initiation-and-growth

(8)

where $\epsilon_{\varphi\varphi\pi}$ is the strain at the end of the primary creep in %; and $\Delta\epsilon_S$ is creep strain increment in %. C_1 , C_2 , and n_1 are material constants which are the same as in Eq. (6); t_{fp} is the end of primary creep time in hour, which calculated as below:

Hosted file

`image19.emf` available at https://authorea.com/users/374572/articles/492073-effect-of-creep-fatigue-loading-condition-on-crack-tip-fields-of-grade-91-steel-at-crack-initiation-and-growth

(9)

where C_3 =2.8690 x 10^{17};n_3 =-6.9531.

The above creep constitutive model was implemented within ABAQUS using the CREEP user-subroutine [43].

4. RESULTS

4.1 Load-Load Line Displacement Results

The creep-fatigue crack growth tests of Grade 91 at 600°C were simulated using the FE analysis method described in Section 3.1 with the material models given in Sections 3.2 and 3.3.

The simulated load-line displacement results are compared with the experimental data in Fig. 6. It shows that, regardless of the cyclic hardening model used, all FE analysis results are very close and are overall in good agreement with experimental data. It shows that deformation behavior of Grade 91 at 600°C under creep-fatigue loading can be well simulated, provided appropriate creep strain model is chosen. The reason is that creep deformation is more dominant than plastic deformation in all cases; creep deformation occurs globally but the plastic deformation is concentrated only near the crack tip (this will be presented in Section 4.2). In the subsequent sub-sections, the combined hardening model by Saad et al. [48] which is closest to experimental result shown in Fig. 5 is used as representative model for FE analysis among the three hardening models, and only the results using the combined hardening model by Saad et al. [48] will be presented.

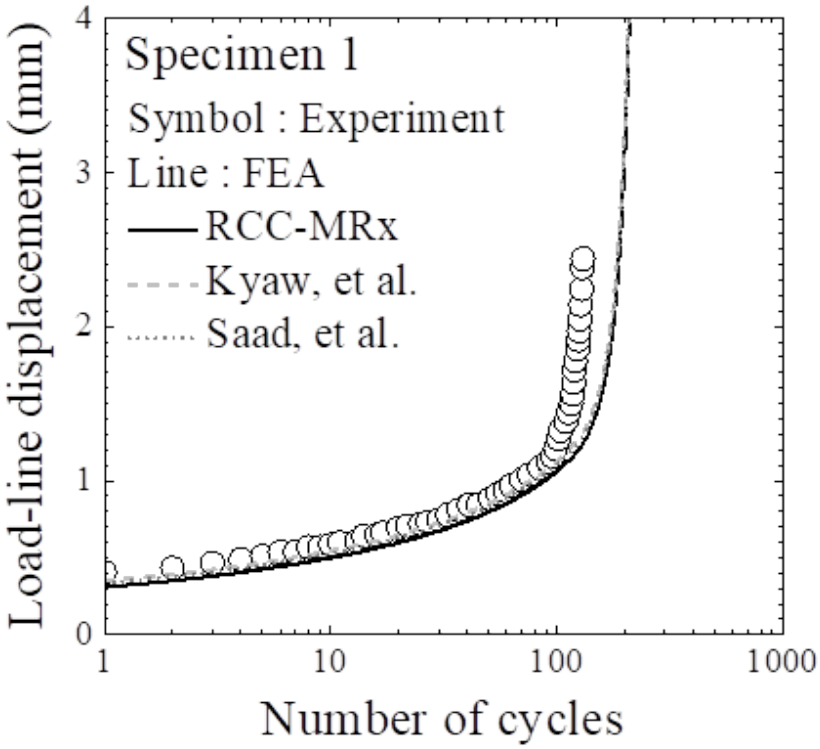

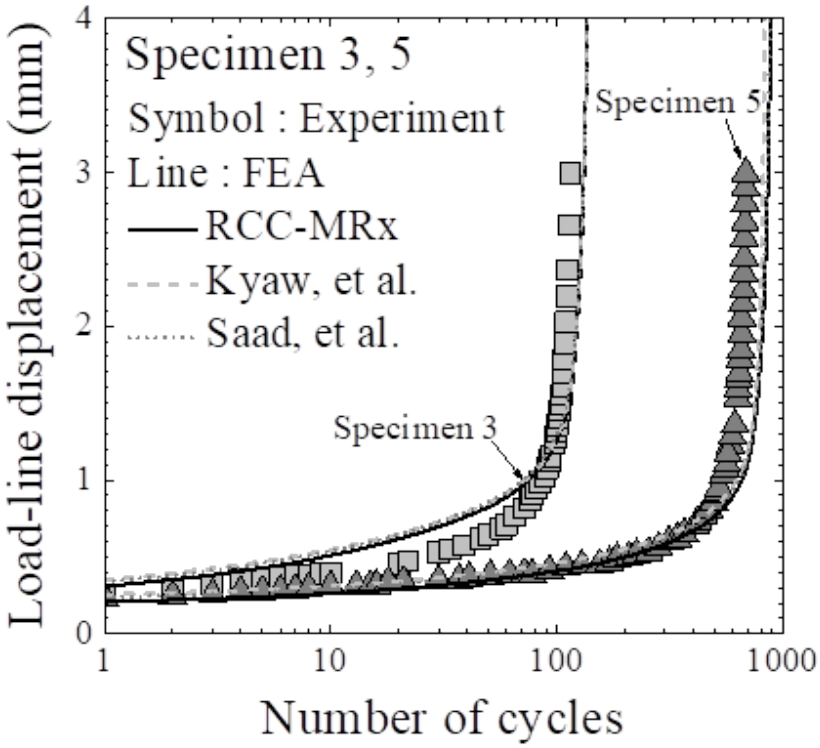

(a) (b)

Figure 6. Load-line displacement versus number of cycles from experiment and FE analysis: (a) specimen 1 and (b) specimen 3 and 5.

4.2 Plastic and Creep Zone Sizes

The effect of creep-fatigue loading conditions (the load ratio $R$and the hold time t_h) on the plastic and creep zone sizes at the crack initiation (Δa = 0 mm) and growth (Δa = 2 mm) is presented in this sub-section. The regions for showing the plastic and creep zone are shown in Fig. 7.

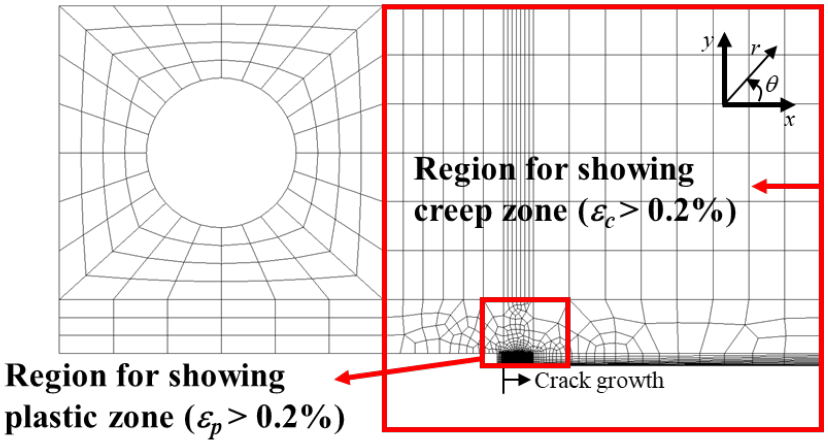

Figure 7. Regions for showing plastic and creep zone

The effect of the load ratio (R) and hold time (t_h) on the plastic zone size are shown in Fig. 8. The contours in Fig. 8 indicates the plastic zone where the equivalent plastic strain is greater than 0.2 %. Both at initiation (Δa = 0 mm) and growth (Δa = 2 mm), the plastic zone size is dependent mainly on the load ratio, whereas the hold time effect is minimal.

Corresponding results for the creep zone size are shown in Fig. 9. The contours in Fig. 9 indicates the creep zone where the equivalent creep strain is greater than 0.2 %. At initiation (Δa = 0 mm), the creep zone size under tension-compression loading (R < 0) is much smaller than that under tension-tension loading (R > 0), and the creep zone size becomes larger with the longer hold time. The same tendency is observed at crack growth (Δa = 2 mm), but the effect of the load ratio becomes weaker and the effect of the hold time is more dominant than that of the load ratio at crack growth.

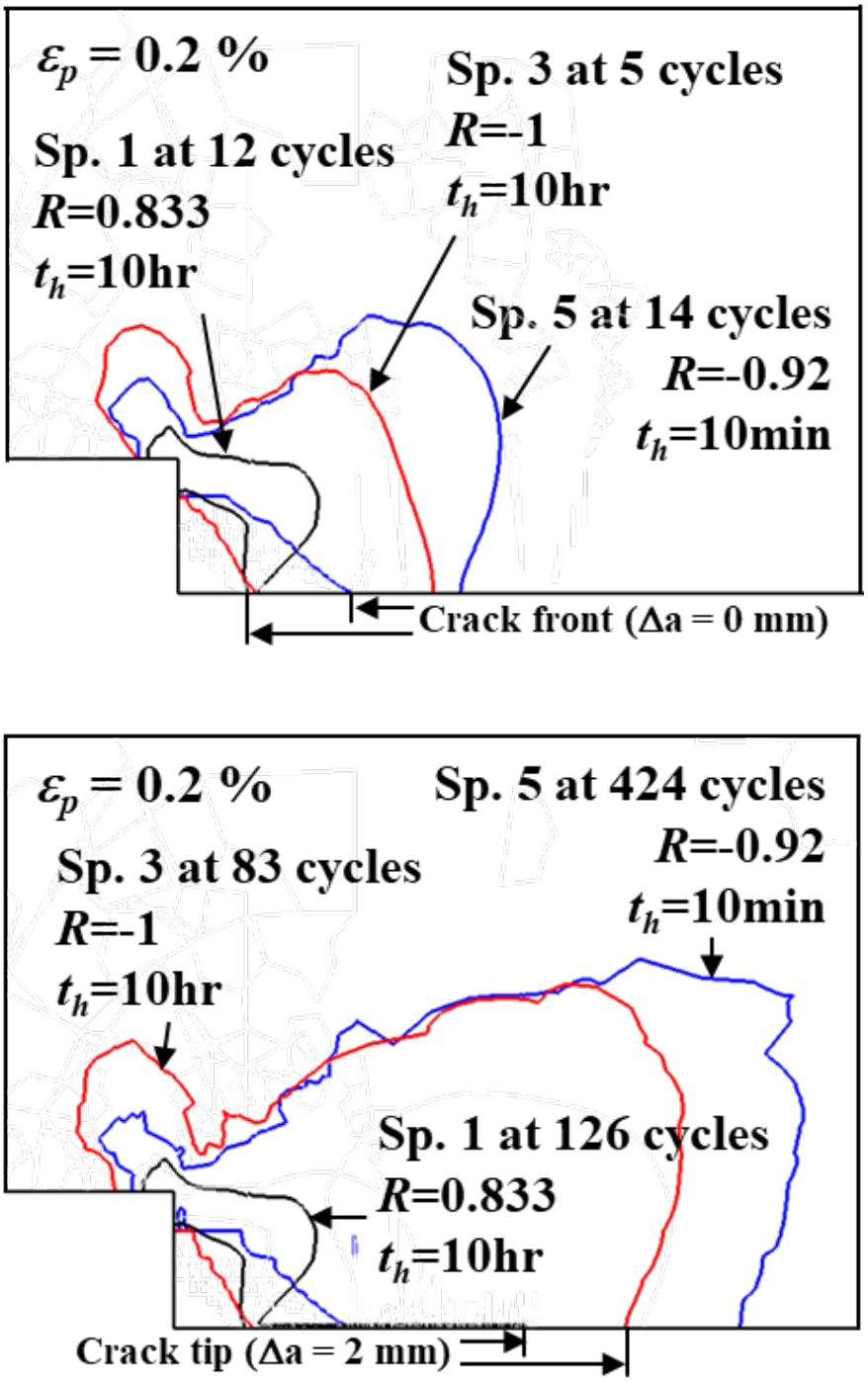

(a) (b)

Figure 8. Effect of loading condition on the plastic zone size: (a) at Δa = 0mm and (b) at Δa = 2mm.

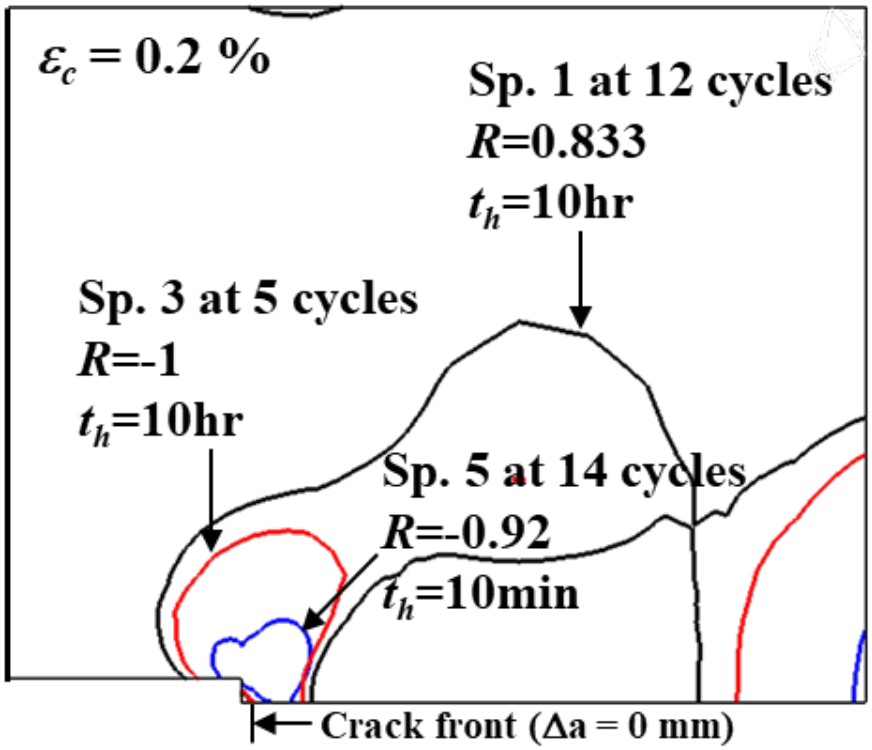

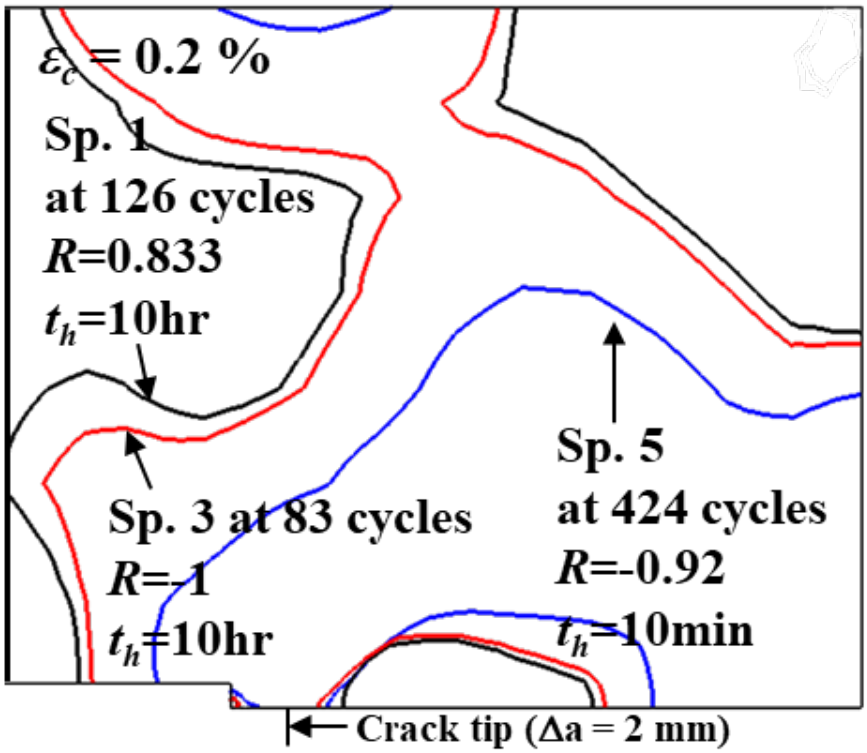

(a) (b)

Figure 9. Effect of loading condition on creep zone size: (a) at Δa = 0mm and (b) at Δa = 2mm

4.3 Crack Opening Profiles

The effect of creep-fatigue loading condition on the crack opening profile is shown in Fig. 10. The crack-opening displacement in Fig. 10 is defined as the half of the vertical displacement of the crack surface (considering the symmetry). When the crack opening displacement becomes zero, it suggests the crack closure. Figures 10(a) and (c) show the crack-opening displacement under the maximum load ($P = P_{max}$) at Δa = 0 mm and Δa = 2 mm, respectively, whereas Figs. 10(b) and (d) show the crack-opening displacement under the minimum load ($P = P_{min}$) at Δa = 0 mm and Δa = 2 mm, respectively.

At initiation (Δa = 0 mm), crack blunting occurs at the maximum load in all cases, as shown in Fig. 10(a). The most blunting occurs for the specimen 1 (R = 0.833 and t_h = 10 hrs), and blunting is depressed with decreasing the load ratio and hold time. As shown in Fig. 10(b), crack closure is observed only in the specimen 5 (R = -0.92 and t_h = 10 min).

At crack growth (Δa = 2 mm), a large difference in the crack opening profile between tension-tension and tension-compression loading is observed. For the tension-compression loading cases (specimen 3 and 5), both crack blunting and closure occur, as shown in Figs. 10(c) and (d). On the other hand, in tension-tension loading case (specimen 1), the sharper crack profile is maintained during loading and unloading cycles.

As the specimen is unloaded and re-loaded elastically for the tension-tension loading, the crack opening profile changes only slightly during loading and unloading and thus the crack growth behavior is similar to that under pure creep loading. On the other hand, the crack growth behavior under the tension-compression creep-fatigue loading is quite different from that under the pure creep loading. The crack closure occurs under compressive loading, which initializes creep-redistributed crack-tip stress states, re-activates the transient deformation, and as a result, the crack blunting occurs.

Hosted file

`image27.emf` available at https://authorea.com/users/374572/articles/492073-effect-of-creep-fatigue-loading-condition-on-crack-tip-fields-of-grade-91-steel-at-crack-initiation-and-growth

Hosted file

`image28.emf` available at https://authorea.com/users/374572/articles/492073-effect-of-creep-fatigue-loading-condition-on-crack-tip-fields-of-grade-91-steel-at-crack-initiation-and-growth

(a) (b)

Hosted file

`image29.emf` available at https://authorea.com/users/374572/articles/492073-effect-of-creep-fatigue-loading-condition-on-crack-tip-fields-of-grade-91-steel-at-crack-initiation-and-growth

Hosted file

`image30.emf` available at https://authorea.com/users/374572/articles/492073-effect-of-creep-fatigue-loading-condition-on-crack-tip-fields-of-grade-91-steel-at-crack-initiation-and-growth

(c) (d)

Figure 10. Effect of loading condition on crack opening profile: (a) at loading ($P = P_{max}$) and Δa = 0mm, (b) at unloading ($P = P_{min}$) and Δa = 0mm, (c) at loading ($P = P_{max}$) and Δa = 2mm and (d) at unloading ($P = P_{min}$) and Δa = 2mm

4.4 Variation of Equivalent Stress Ahead of the Crack Tip

The effect of the creep-fatigue loading condition on the equivalent stress distribution at the maximum load ($P = P_{max}$) is shown in Fig. 11. At initiation (Δa = 0 mm), equivalent stresses near crack tip in all cases are almost same as shown in Fig. 11(a), but with increasing the distance from the crack tip, the equivalent stress for the tension-tension loading case (specimen 1) decreases more rapidly than that for the tension-compression loading case (specimen 3 and 5).

At growth (Δa = 2 mm), the equivalent stress for the tension-compression loading case is overall higher than that for the tension-tension loading case, as shown in Fig. 11(b). It is because of the crack closure under compressive loading, which initializes stress relaxation by creep; under the tension-tension loading, initially creep-relaxed stress distribution is maintained during crack growth. High equivalent stress at growth under tension-compression loading causes rapid creep deformation, which is previously reported as re-activation of transient creep deformation by Takahashi [28]. Meanwhile, both at initiation and growth (Δa = 2 mm), the hold time rarely affects the equivalent stress distribution.

Hosted file

`image31.emf` available at https://authorea.com/users/374572/articles/492073-effect-of-creep-fatigue-loading-condition-on-crack-tip-fields-of-grade-91-steel-at-crack-initiation-and-growth

Hosted file

`image32.emf` available at https://authorea.com/users/374572/articles/492073-effect-of-creep-fatigue-loading-condition-on-crack-tip-fields-of-grade-91-steel-at-crack-initiation-and-growth

(a) (b)

Figure 11. Effect of loading condition on equivalent stress field at maximum load ($P = P_{max}$): (a) at Δa = 0mm and (b) at Δa = 2mm

4.5 Variation of Stress Triaxiality Ahead of the Crack Tip

Hosted file

`image33.emf` available at https://authorea.com/users/374572/articles/492073-effect-of-creep-fatigue-loading-condition-on-crack-tip-fields-of-grade-91-steel-at-crack-initiation-and-growth

Hosted file

`image34.emf` available at https://authorea.com/users/374572/articles/492073-effect-of-creep-fatigue-loading-condition-on-crack-tip-fields-of-grade-91-steel-at-crack-initiation-and-growth

(a) (b)

Figure 12. Effect of loading condition on stress triaxiality field at maximum load ($P = P_{max}$): (a) at Δa = 0mm and (b) at Δa = 2mm

The effect of the creep-fatigue loading condition on the stress triaxiality is shown in Fig. 12. At initiation (Δa = 0 mm), not much difference can be seen between three test cases, as shown in Fig. 12(a). However, at growth (Δa = 2 mm), the stress triaxiality of the tension-tension loading case (specimen 1) is the highest,

and that of the tension-compression loading with the short hold time (specimen 5) is the lowest, as shown in Fig. 12(b). The effect of the hold time on the stress triaxiality is not so significant.

Takahashi [28] has reported from experimental data of Grade 91 steel that the predicted crack growth rates using the C^* parameter were overly conservative for the tension-compression creep-fatigue case. This may be because that the low stress triaxiality induced by crack blunting under tension-compression loading condition can increase resistance for crack growth, compared to the cases of the tension-tension loading and pure creep condition. This will be discussed further in the next sub-section.

4.6 Characterization of Crack-tip Stress Fields using Fracture Mechanics Parameters

Crack tip hoop stresses calculated from the FE analysis under creep-fatigue loading are compared with analytical crack tip stresses from RR (Riedel and Rice) fields [18] which are the C *-controlled crack-tip stress fields under steady state creep conditions for a power-law creep material. The stress fields are given by

Hosted file

`image35.emf` available at https://authorea.com/users/374572/articles/492073-effect-of-creep-fatigue-loading-condition-on-crack-tip-fields-of-grade-91-steel-at-crack-initiation-and-growth

(11)

where (r , ϑ) are the polar coordinate at the crack-tip;$\tilde{\sigma}_{\mathrm{ij}}$ is a dimensionless stress function depending on m or n and $\vartheta \cdot$ for Grade 91 at 600°C considered in this paper,σ_0 =311 MPa; $a\epsilon_0$ =0.002;$\dot{\varepsilon}_0$ = 6.47x10^{-3} 1/h; n =7.63; and the integration constant I_n =4.66 for n =7.63. Based on the reference stress approach [50], the fracture mechanics parameters C^* can be calculated using

Hosted file

`image36.emf` available at https://authorea.com/users/374572/articles/492073-effect-of-creep-fatigue-loading-condition-on-crack-tip-fields-of-grade-91-steel-at-crack-initiation-and-growth

(13)

where reference stress $\sigma_{\rho\epsilon\varphi}$ is defined by the plastic limit load P_o ,$\sigma_{\rho\epsilon\varphi}$ =σ_0 (P/P_0);$\varepsilon^p_{\mathrm{ref}}$ and$\dot{\varepsilon}^c_{\mathrm{ref}}$ are the reference plastic strain and reference creep strain rate at the corresponding reference stress, respectively; and K is the stress intensity factor.

The crack-tip hoop stresses at the maximum load and the end of hold time are compared with the RR stress in Fig. 13 at crack initiation (Δa = 0 mm) and growth (Δa = 2 mm). For the tension-tension loading case (specimen 1), shown in Fig. 13(a) and (b), the crack-tip stresses are slightly changed during the hold time, and are close to the RR stress both at crack initiation and growth. This suggests that the stress field is similar to that under pure creep condition. On the other hand, the tension-compression loading cases (specimen 3 and 5) show quite different crack-tip stresses from that under pure creep condition. For the tension-compression with long hold time (specimen 3), shown in Fig. 13(c) and (d), the crack-tip stresses decrease significantly during the hold time, and the crack-tip stress at the end of hold time is close to the RR stress both at crack initiation and growth. For the tension-compression with short hold time (specimen 5), shown in Fig. 13(e) and (f), the crack-tip stress remains similar during hold time and is much higher than the RR stress both at crack initiation and growth. The difference between tension-tension and tension-compression loading condition arises from initialization of the creep-relaxed stress caused by compressive loading, which is mentioned in Section 4.4. Furthermore, for tension-compression cases (specimen 3 and 5), the hoop stresses near the crack tip are close to or lower than the RR stress, due to formation of local creep-dominant zone, cyclic softening, and large deformation of crack tip (blunting). The effect of the cyclic softening is appreciable in the specimen 5 at crack growth, as shown in Fig. 13(f).

Hosted file

image37.emf available at https://authorea.com/users/374572/articles/492073-effect-of-creep-fatigue-loading-condition-on-crack-tip-fields-of-grade-91-steel-at-crack-initiation-and-growth

Hosted file

image38.emf available at https://authorea.com/users/374572/articles/492073-effect-of-creep-fatigue-loading-condition-on-crack-tip-fields-of-grade-91-steel-at-crack-initiation-and-growth

(a) (b)

Hosted file

image39.emf available at https://authorea.com/users/374572/articles/492073-effect-of-creep-fatigue-loading-condition-on-crack-tip-fields-of-grade-91-steel-at-crack-initiation-and-growth

Hosted file

image40.emf available at https://authorea.com/users/374572/articles/492073-effect-of-creep-fatigue-loading-condition-on-crack-tip-fields-of-grade-91-steel-at-crack-initiation-and-growth

(c) (d)

Hosted file

image41.emf available at https://authorea.com/users/374572/articles/492073-effect-of-creep-fatigue-loading-condition-on-crack-tip-fields-of-grade-91-steel-at-crack-initiation-and-growth

Hosted file

image42.emf available at https://authorea.com/users/374572/articles/492073-effect-of-creep-fatigue-loading-condition-on-crack-tip-fields-of-grade-91-steel-at-crack-initiation-and-growth

(e) (f)

Figure 13. Comparison of crack-tip hoop stresses at the maximum load and the end of hold time with the RR fields at crack initiation ($\Delta a = 0$ mm) and growth ($\Delta a = 2$ mm): (a)-(b) specimen 1, (c)-(d) specimen 3 and (e)-(f) specimen 5.

5. CONCLUSION

In this paper, the effect of various creep-fatigue loading conditions on crack-tip fields are investigated via the FE debond analysis using experimental creep-fatigue test data of Grade 91 steel at 600°C. The following conclusions are drawn:

The crack-tip deformation and stress fields during crack growth under tension-compression creep-fatigue loading is overall different from those under the tension-tension creep fatigue and pure creep loading, due to crack closure. The crack closure under compressive loading initializes creep-redistributed stress states, re-activates transient creep deformation, promotes crack-tip blunting and reduces the stress triaxiality. This is the reason that the predicted crack growth rates using the C^* parameter were overly conservative for the tension-compression creep-fatigue case.

For the tension-tension creep-fatigue case, the crack-tip stresses can be well characterized by the C^* parameter both at crack initiation and at crack growth, whereas those under tension-compression creep-fatigue

loading cannot be correlated either with C^* parameter. To characterize the crack-tip stress field under tension-compression creep-fatigue loading, the effects of local creep-dominant zone and cyclic softening should be considered.

ACKNOWLEDGMENT

This research was supported by National Research Foundation of Korea (NRF) funded by the Ministry of Science, ICT and Future Planning (NRF-2017R1A2B2009759).

REFERNECE

1. Riedel H. Creep Crack Growth. *ASTM STP 1020* . USA: ASTM; 1989:101-126. https://doi.org/10.1520/STP18822S
2. Hollstein T, Webster GA, Djavanroodi F. Creep crack growth in a 1%CrMoV steel and a 32%Ni-20%Cr alloy. *Mater High Temp.*1992;10(2):92-96. https://doi.org/10.1080/09603409.1992.11689406
3. Maile K, Schellenberg G, Granacher J and Tramer M. Description of creep and creep fatigue crack growth in 1% and 9% Cr steels.*Mater High Temp.* 1998;15(2):131-137. https://doi.org/10.1080/09603409.1998.11689591
4. Dogan B, Petrovski B. Creep crack growth of high temperature weldments. *Int J Pres Ves Pip.* 2001;78:795-805. https://doi.org/10.1016/S0308-0161(01)00092-8
5. Shibli IA, Hamata MLM. Creep crack growth in P22 and P91 welds – overview from SOTA and HIDA projects. *Int J Pres Ves Pip.*2001;78:785-793. https://doi.org/10.1016/S0308-0161(01)00091-6
6. Hamata MLM, Shibli IA. Creep crack growth of seam-welded P22 and P91 pipes with artificial defects - Part I. Experimental study and post-test metallography. *Int J Pres Ves Pip.* 2001;78:819-826. https://doi.org/10.1016/S0308-0161(01)00096-5
7. Hamata MLM, Shibli IA. Creep crack growth of seam-welded P22 and P91 pipes with artificial defects - Part II. Data analysis. *Int J Pres Ves Pip.* 2001;78:827-835. https://doi.org/10.1016/S0308-0161(01)00097-7
8. Hyde TH, Saber M, Sun W. Testing and modelling of creep crack growth in compact tension specimen from a P91 weld at 650°C. *Eng Fract Mech.* 2010;77:2946-2957. https://doi.org/10.1016/j.engfracmech.2010.03.043
9. Hyde TH, Saber M, Sun W. Creep crack growth data and prediction for a P91 weld at 650°C. *Int J Pres Ves Pip.*2010;87:721-729. https://doi.org/10.1016/j.ijpvp.2010.09.002
10. Yamamoto M, Miura N, Ogata T. Applicability of C^*parameter in assessing Type IV creep cracking in Mod. 9Cr–1Mo steel welded joint. *Eng Fract Mech.* 2010;77:3022-3034. https://doi.org/10.1016/j.engfracmech.2010.04.023
11. Ohji K, Ogura K, Kubo S. Creep crack propagation rate in SUS 304 stainless steel and interpretation in Terms of Modified J-Integral.*T Jpn Soc Mech Eng.* 1976;42:350-358.
12. Webster GA, Ainsworth RA. *High temperature component life assessment* . UK: Champman & Hall; 1994.
13. Landes JD, Begley JA. A fracture mechanics approach to creep crack growth. *ASTM STP 590* . USA: ASTM; 1976:128-148. https://doi.org/10.1520/STP33943S
14. Nikbin KM, Webster GA, Turner CE. Relevance of nonlinear fracture mechanics to creep crack growth. *ASTM STP 601* . USA: ASTM; 1976:47-62. https://doi.org/10.1520/STP28637S
15. Ainsworth RA. The initiation of creep crack growth. *Int J Solids Struct.* 1982;18:873-881. https://doi.org/10.1016/0020-7683(82)90071-3
16. Piques R, Molinie E, Pineau A. Comparison between two assessment methods for defects in the creep range. *Fatigue Fract Eng Mater Struct.* 1991;14:871-885. https://doi.org/10.1111/j.1460-2695.1991.tb00721.x
17. Anderson TL. *Fracture mechanics: fundamentals and applications* . USA: Taylor & Francis - CRC Press; 2005.
18. Riedel H, Rice JR. Tensile crack in creeping solids. *ASTM STP 700* . USA: ASTM; 1980:112-130. https://doi.org/10.1520/STP36967S

19. Taira S, Ohtani R, Kitamura T, Yamada K. J-integral approach to crack propagation under combined creep and fatigue condition. *TJpn Soc Mater Sci.* 1979;28:414–420.
20. Ohji K, Kubo S. Fatigue crack propagation behavior under creep conditions. In: *Creep in structures: 4th IUTAM Symposium (Part II)* . Germany: Springer; 1991:253–268. https://doi.org/10.1007/978-3-642-84455-3_30
21. Grover PS, Saxena A. Modelling the effect of creep-fatigue interaction on crack growth. *Fatigue Fract Eng Mater Tech.*1999;22:111–122. https://doi.org/10.1046/j.1460-2695.1999.00144.x
22. Granacher J, Klenk A, Tramer M, Schellenberg G, Mueller F, Ewald J. Creep fatigue crack behavior of two power plant steels. *Int J Pres Ves Pip* . 2001;78:909-920. https://doi.org/10.1016/S0308-0161(01)00106-5
23. Lu YL, Chen LJ, Liaw PK, Wang GY, Brooks CR, Thompson SA, et al. Effects of temperature and hold time on creep-fatigue crack-growth behavior of HAYNES® 230® alloy.*Mater Sci Eng A* . 2006;429:1-10. https://doi.org/10.1016/j.msea.2005.07.039
24. Mehmanparast A, Davies CM, Nikbin KM. Evaluation of the testing and analysis methods in ASTM E2760-10 creep-fatigue crack growth testing standard for a range of steels. *ASTM STP 1539* . USA: ASTM; 2011:41-66. https://doi.org/10.1520/STP49934S
25. Holdsworth S. Creep-fatigue interaction in power plant steels.*Mater High Temp* . 2011;28(3): 197-204. https://doi.org/10.3184/096034011X13123676561681
26. Narasimhachary SB, Saxena A. Crack growth behavior of 9Cr-1Mo (P91) steel under creep-fatigue conditions. *Int J Fatigue.*2013;56:106–113. https://doi.org/10.1016/j.ijfatigue.2013.07.006
27. Bassi F, Foletti S, Conte AL. Creep fatigue crack growth and fracture mechanisms of T/P91 power plant steel. *Mater High Temp* . 2015;32(3):250-255. https://doi.org/10.1179/0960340914Z.00000000065
28. Takahashi Y. Effect of intermittent unloading or reversed loading on high temperature crack growth behaviour of Grade 91 steel under constant tensile load. *Mater High Temp.* 2015;32(3):256-265. https://doi.org/10.1179/0960340914Z.00000000066
29. Razak NA, Davies CM, Nikbin KM. Creep-fatigue crack growth behaviour of P91 steels. *Proc Struct Integr* . 2016;2:855-862. https://doi.org/10.1016/j.prostr.2016.06.110
30. Guerra-Rosa L, Branco CM, Randon JC. Monotonic and cyclic crack tip plasticity. *Int J Fatigue* . 1984;6:17-24. https://doi.org/10.1016/0142-1123(84)90004-5
31. Pommier S. Plane strain crack closure and cyclic hardening. *Eng Fract Mech.* 2002;69:25-44. https://doi.org/10.1016/S0013-7944(01)00061-3
32. Wang CH, Rose LRF, Newman Jr. JC. Closure of plane-strain cracks under large-scale yielding conditions. *Fatigue Fract Eng Mater Struct.* 2002;25:127-139. https://doi.org/10.1046/j.8756-758x.2002.00483.x
33. Zhao LG, Tong J, Byrne J. The evolution of the stress–strain fields near a fatigue crack tip and plasticity-induced crack closure revisited. *Fatigue Fract Eng Mater Struct.* 2004;27:19-29. https://doi.org/10.1111/j.1460-2695.2004.00716.x
34. Toribio J, Kharin V. Finite-deformation analysis of the crack-tip fields under cyclic loading. *Int J Solids Struct.*2009;46(9):1937-1952. https://doi.org/10.1016/j.ijsolstr.2009.01.006
35. Paul SK, Tarafder S. Cyclic plastic deformation response at fatigue crack. *Int J Pres Ves Pip.* 2013;101:81-90. https://doi.org/10.1016/j.ijpvp.2012.10.007
36. Jingjie C, Yi H, Leilei D, Yugang L. A new method for cyclic crack-tip plastic zone size determination under cyclic tensile load. *Eng Fract Mech.* 2014;126:141-154. https://doi.org/10.1016/j.engfracmech.2014.05.001
37. Paul SK. Numerical models of plastic zones and associated deformations for a stationary cr ack in a C(T) specimen loaded at different R-ratios. *Eng Fract Mech.* 2016;152:72-80. https://doi.org/10.1016/j.engfracmech.2015.12.008
38. Jiang W, Yu Y, Zhang W, Xiao C,Woo W. Residual stress and stress fields change around fatigue crack tip: Neutron diffraction measurement and finite element modelling. *Int J Pres Ves Pip.*2020;179:104024. https://doi.org/10.1016/j.ijpvp.2019.104024
39. Hwang JH, Kim HT, Kim YJ, Nam HS, Kim JW. Crack tip fields at crack initiation and growth

under monotonic and large amplitude cyclic loading: Experimental and FE analyses. *Int J Fatigue.*2020;141:105889. https://doi.org/10.1016/j.ijfatigue.2020.105889

40. Standard specification for pressure vessel plates, alloy steel, chromium-molybdenum (A387/A387M). In: *ASTM Volume 01.04 - ASTM steel structural, reinforcing, pressure vessel, railway* . USA: ASTM; 2014.
41. Flat products made of steels for pressure purposes – Part 2: Non-alloy and alloy steels with specified elevated temperature properties (BS EN10028-2). UK: British Standard Institution; 2009.
42. Kumar V, German MD, Shih CF. Engineering approach for elastic-plastic fracture analysis (EPRI-NP—1931). USA: General Electric Cooperative, 1981.
43. Abaqus version 2018 manual. France: Dassault Systems; 2015.
44. Properties Groups for products and parts in alloy steel grade X10CrMoVNb9-1 normalised - tempered or quenched – tempered (Appendix A3.18AS). In: *RCC-MRx Section III – Tome 1 – Subsection Z* . France: AFCEN; 2010.
45. Chaboche JL, Van KD, Cordier G. Modelization of the strain memory effect on the cyclic hardening of 316 stainless steel. In: *Proc. of the 5th International Conference on 'Structural Mechanics in Reactor Technology Div. L* . USA: North-Holland Publishing Company for the Commission of the European Communities; 1979.
46. Chaboche JL. Time-independent constitutive theories for cyclic plasticity. *Int J Plasticity.* 1986;2(2):149-188. https://doi.org/10.1016/0749-6419(86)90010-0
47. Kyaw ST, Rouse JP, Lu J, Sun W. Determination of material parameters for a unified viscoplasticity-damage model for a P91 power plant steel. *Int J Mech Sci* . 2016;115-116:168-179. https://doi.org/10.1016/j.ijmecsci.2016.06.014
48. Saad AA, Hyde CJ, Sun W, Hyde TH. Thermal-mechanical fatigue simulation of a P91 steel in a temperature range of 400–600degC.*Mater High Temp* . 2011;28(3):212-218. https://doi.org/10.3184/096034011X13072954674044
49. Yaguchi M, Takahashi Y. Development of inelastic constitutive equations for modified 9Cr-1Mo steel (No. T97034). Japan: Central Research Institute of Electric Power Industry, Tokyo, Japan; 1998.
50. Ainsworth RA. The assessment of defects in structures of strain hardening material. *Eng Fract Mech* . 1984;19:633-642. https://doi.org/10.1016/0013-7944(84)90096-1